

Incorporating metal active centers to Covalent Organic Framework for Boosting CO₂ Photoreduction

Ming-zhen Chen^{a,#}, Hai-rong Zhao^{b,#}, Kai-ming Zhang^c, Hong-jing Zhu^b, Hai-bao Duan^{b*}, Xiao-Ming Ren^{a*}

^a School of Chemistry and Molecular Engineering, Nanjing Tech University, Nanjing 211816, China

^b School of Environmental science, Nanjing Xiaozhuang University, Nanjing 210009, P. R. China.

^c Department of material science and engineering, Nanjing Institute of Technology, Nanjing 211167, P. R. China.

E-mail: duanhaibao4660@163.com; Tel: +86 25 13814001884

These authors contributed equally: Ming-zhen Chen and Hai-rong Zhao

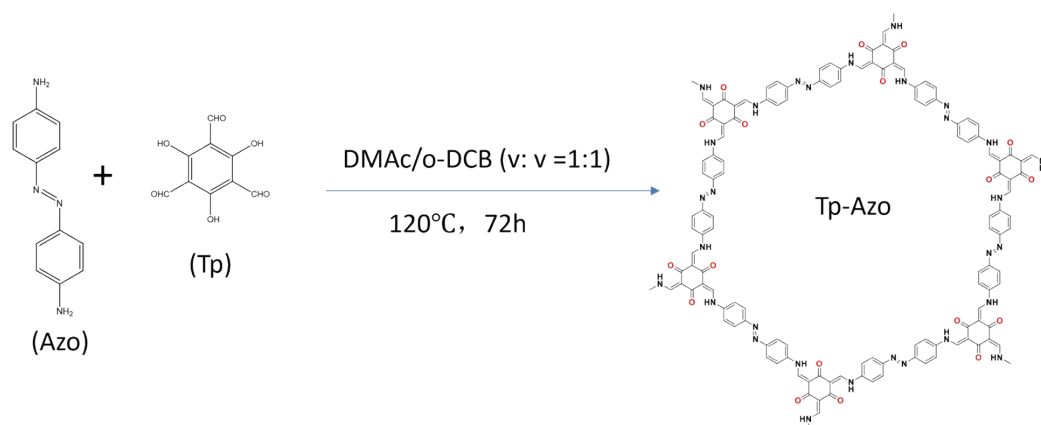
1. Experiment

1.1 Chemicals

2,4,6-trihydroxybenzene-1,3,5-tricarbaldehyde (Tp, 97%, Macklin), 4,4'-Azodiphenylamine (Azo, $\geq 98\%$, Macklin), 1,2-Dichlorobenzene (98%, Macklin), N,N-Dimethylacetamide (99.0%, Macklin), nickel acetate tetrahydrate ($\text{Ni}(\text{OAc})_2 \cdot 4\text{H}_2\text{O}$) and Ethyl Alcohol (AR) were purchased from Sinopharm Group Company Limited, Acetonitrile ($\geq 99.5\%$, GC, Macklin), Trithanolamine (TEOA, $\geq 99\%$, GC, Macklin), All chemicals and reagents are used directly without further purification, $[\text{Ru}(\text{2,2}'\text{-bipyridine})_3]\text{Cl}_2 \cdot 6\text{H}_2\text{O}$ (98.0%, Macklin), Nafion solution (5 wt%, Macklin).

1.2 Synthesis of COF-Tp-Azo

Triformyl-phloroglucinol (Tp) (0.063 g, 0.3 mmol), 4,4'-azodiphenylamine (0.095 g, 0.45 mmol), 3 mL N, N-dimethylacetamide and 3 mL 1,2-Dichlorobenzene were added to Pyrex tubes. The mixture was ultrasounded for 10 minutes to get an even dispersion. The tube was then rapidly frozen at 77 K (liquid N_2 bath) and degassed through three freezing pump thawing cycles. Seal the tubes and heat them in a 120 °C oven for 3 days. A dark red precipitate is collected by centrifugation or filtration and washed with THF and acetone. After drying at 100 °C under vacuum for 12 h, pure red powder solid was obtained.



1.3 Loading of Ni(II) into COF-Tp-Azo

The Tp-Azo covalent organic framework (100 mg) and $\text{Ni}(\text{OAc})_2 \cdot 4\text{H}_2\text{O}$ (2.49 g, 0.08 mol) were added to water (100 mL). After ultrasonic treatment for about 20 min to ensure complete dissolution of nickel acetate, the mixture was heated and reflow

for 72 h. The solution is then cooled to room temperature and filtered. Wash thoroughly with water and ethanol to remove free metal ions. The final is dried overnight at 100 °C under a dynamic vacuum to obtain Tp-Azo-Ni.

1.4 Material characterization

The crystallinity of prepared sample Tp-Azo-COF was characterized by powder X-ray diffraction (PXRD) and recorded using using a Bruker D8 Advance X-ray diffractometer at 40 kV and 40 mA over 2° to 50° 2θ range with a Cu Kα radiation. X-ray photoelectron spectroscopy (XPS) measurements were performed on the Thermo Scientific ESCALAB Xi+ electron spectrometer with Al Kα (1486.6 eV) radiation as the X-ray excitation source. Nitrogen adsorption was measured by Micromeritics ASAP 2460 volume adsorption analyzer at 77.3 K. The ultraviolet-visible (UV-Vis) diffuse reflectance spectra (DRS) were obtained by a UV-vis-NIR spectrometer (Shimadzu, UV3600 Plus) equipped with an integrating sphere using BaSO₄ as a reference. Fourier transform infrared (FT-IR) spectra were recorded on the PerkinElmer Spectrum Two in reflection mode, with a range of 400-4000 cm⁻¹. In situ diffuse reflection FTIR spectra were recorded by the Germanicolet iS50 FTIR spectrometer. Field emission scanning electron microscopy (SEM) were performed on the Hitachi SU8100 and ZEISS Gemini SEM 300 with an accelerated voltage of 10.0 kV. Energy Dispersive X-ray (Ultim Max) mapping of X-ray (EDX) elements is performed on a scanning transmission electron microscope. Transmission electron microscopy (TEM) and high-resolution TEM (HRTEM) images were recorded on the JEM-2100F instrument. The steady-state photoluminescence (PL) spectra was measured by HORIBA Fluorolog-3. In the isotope labeling experiment, ¹³CO₂ gas was substituted for ¹²CO₂ gas and H₂¹⁸O was substituted for H₂O. Gas chromatogram-mass spectrometry (GC-MS, Agilent GC/MS-7000D) was used to analyze the gas phase products.

1.5 Photocatalytic measurement

The photocatalytic reduction of carbon dioxide is carried out in a sealable quartz container with a total volume of 100 mL. The reaction vessel contained catalysts 2mg, Ru(bpy)₃Cl₂·6H₂O (0.04 mmol, 22.5 mg), TEOA 2 mL and 15 mL ACN/H₂O (v/v =

4:1), which were uniformly dispersed by ultrasound. The sealed quartz container is then placed in the CEL-PAEM-D8Plus all-glass automatic on-line trace gas analysis system. Vacuum the sample tube with the oil pump and then saturate it with high purity carbon dioxide gas ($\geq 99\%$) to 1 atm. The reaction mixture is continuously stirred with a magnetic stirrer and irradiated under an Xe lamp (CEL-PF300-T6, $\lambda > 420$ nm). Gas chromatographic analysis was conducted using FL9790 II equipped with a flame ionization detector (FID) and a thermal conductivity detector (TCD) column and the carrier gas used was Ar. After the visible light catalytic reduction of CO_2 reaction, the catalyst was recovered by centrifugal separation, washed with acetonitrile, and then vacuum dried, transferred to the reaction system, adding fresh solvent for the next cycle reaction, which has verified the recyclable stability of the catalyst.

1.6 Electrochemistry study

The electrochemical test was carried out on the CHI 760E electrochemical workstation, using a three-electrode system with 0.1 M Na_2SO_4 aqueous solution as the electrolyte, ITO conductive glass as the working electrode, Ag/AgCl electrode as the reference electrode, and Pt electrode as the electrode. The 5 mg COF powder was dispersed and mixed with 30 μl ethanol, 30 μl Nafion and 140 μl aqueous solution, and ultrasonic treatment was performed for 30 minutes. The resulting mixture is evenly dribbled onto the conductive surface of the 1×2 cm^2 area at the bottom of the ITO glass plate, and then placed in the air to dry.

1.7 DFT calculations

Using DFT calculation for energy and structure optimization, using mixed gaussian and plane wave basis set in the QUICKSTEP module CP2K code implementation.¹⁻³ The electron interactions in the system were meticulously described using the generalized gradient approximation (GGA) for the exchange-correlation functional, specifically employing the formulation developed by Perdew, Burke, and Ernzerhof (PBE).⁴ In addition to this foundational method, the core electrons of transition metal atoms were treated with norm-conserving Goedecker-Teter-Hutter pseudopotentials. Furthermore, the wave function corresponding to

valence electrons is extended to double zeta polarization function and auxiliary plane wave base set.⁵⁻⁷ An energy cutoff value of 400 Ry was used in all calculations. The Broyden-Fletcher-Goldfarb-Shanno (BGFS) algorithm is used to optimize the structure of reaction intermediates, which is widely used in nonlinear optimization problems because of its high efficiency and convergence. Meanwhile, in order to ensure the accuracy of self-consistent field (SCF) calculation, 1.0×10^{-6} a.u. was set in this study. As a convergence standard to ensure the stability of the electronic structure. Furthermore, the DFT-D3 scheme is incorporated and the empirical damping potential term is combined when taking into account the long-range dispersive interaction. These meticulous methodological choices make this study have stronger scientific basis and practical value when dealing with complex systems.⁸

In this paper, a computational hydrogen electrode (CHE) model was used to calculate the Gibbs free energy change (ΔG) of each basic step of the CO₂ electroreduction reaction.⁹

$$\Delta G = \Delta E_{elec} + \Delta E_{ZPE} - T\Delta S + \Delta G_{pH} + \Delta G_U \quad (1)$$

Where E_{elec} and E_{ZPE} are the electron term and zero point energy (ZPE) contributions directly calculated by DFT, respectively. S is the entropy, T is the temperature (298.15 K). ΔG_U is the effect of applied electrode potential (U), where $\Delta G_U = -eU$. Define the limit potential (U_L) of CO₂RR as $U_L = -\Delta G_{max}/ne$ and ΔG_{max} as the Gibbs free energy change of the set step (PDS). E_{ZPE} and TS can be calculated as follows:¹⁰

$$E_{ZPE} = \frac{1}{2} \sum_i h\nu_i \quad (2)$$

$$-TS = k_B T \sum_i \ln \left(1 - e^{-\frac{h\nu_i}{k_B T}} \right) - \sum_i h\nu_i \left(\frac{1}{e^{\frac{h\nu_i}{k_B T}} - 1} \right) \quad (3)$$

Where k_B is the Boltzmann constant, h is the Planck's constant, and ν_i is the vibration frequency. The vibration frequency is calculated using the local harmonic oscillator

approximation with A displacement of 0.01 Å. In the vibration frequency calculation, only the reaction intermediate is relaxed, while the other atoms of the frame are fixed.

References:

- (1) M. Krack and M. Parrinello, All-electron *ab-initio* Molecular Dynamics, *Phys. Chem. Chem. Phys.*, 2000, **2**, 2105-2112.
- (2) T. D. Kühne, M. Iannuzzi, M. Del Ben, V. V. Rybkin, P. Seewald, F. Stein, T. Laino, R. Z. Khaliullin, O. Schütt, F. Schiffmann, D. Golze, J. Wilhelm, S. Chulkov, M. H. Bani-Hashemian, V. Weber, U. Borštnik, M. Taillefumier, A. S. Jakobovits, A. Lazzaro, H. Pabst, T. Müller, R. Schade, M. Guidon, S. Andermatt, N. Holmberg, G. K. Schenter, A. Hehn, A. Bussy, F. Belleflamme, G. Tabacchi, A. Glöß, M. Lass, I. Bethune, C. J. Mundy, C. Plessl, M. Watkins, J. VandeVondele, M. Krack and J. Hutter, CP2K: An Electronic Structure and Molecular Dynamics Software Package-Quickstep: Efficient and Accurate Electronic Structure Calculations, *J. Chem. Phys.*, 2020, **152**, 194103.
- (3) J. VandeVondele, M. Krack, F. Mohamed, M. Parrinello, T. Chassaing and J. Hutter, Quickstep: Fast and Accurate Density Functional Calculations Using a Mixed Gaussian and Plane Waves Approach, *Comput. Phys. Commun.*, 2005, **167**, 103-128.
- (4) J. P. Perdew and K. Burke, Generalized Gradient Approximation Made Simple, *Phys. Rev. Lett.*, 1996, **77**, 3865.
- (5) J. VandeVondele and J. Hutter, Gaussian Basis Sets for Accurate Calculations on Molecular Systems in Gas and Condensed Phases, *J. Chem. Phys.*, 2007, **127**, 114105.
- (6) S. Goedecker, M. Teter and J. Hutter, Separable Dual-Space Gaussian Pseudopotentials, *Phys. Rev. B*, 1996, **54**, 1703-1710.
- (7) C. Hartwigsen, S. Goedecker and J. Hutter, Relativistic Separable Dual-Space Gaussian Pseudopotentials from H to Rn, *Phys. Rev. B*, 1998, **58**, 3641-3662.
- (8) S. Grimme, J. Antony, S. Ehrlich and H. Krieg, A Consistent and Accurate *ab initio* Parametrization of Density Functional Dispersion Correction (DFT-D) for the 94 Elements H-Pu, *J. Chem. Phys.*, 2010, **132**, 154104.
- (9) J. Rossmeis, Z. W. Qu, H. Zhu, G. J. Kroes and J. K. Nørskov, Electrolysis of Water on Oxide Surfaces, *J. Electroanal. Chem.*, 2007, **607**, 83-89.
- (10) C.-Y. Ling, X.-H. Niu, Q. Li, A.-J. Du and J.-L. Wang, Metal-Free Single Atom Catalyst for N₂ Fixation Driven by Visible Light, *J. Am. Chem. Soc.*, 2018, **140**, 14161-14168.

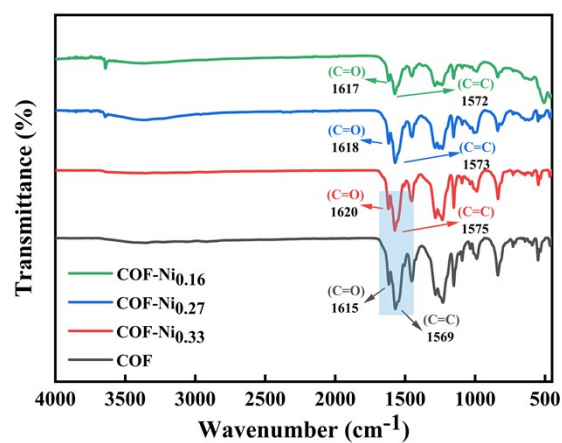


Figure S1. In situ FTIR spectra experiments.

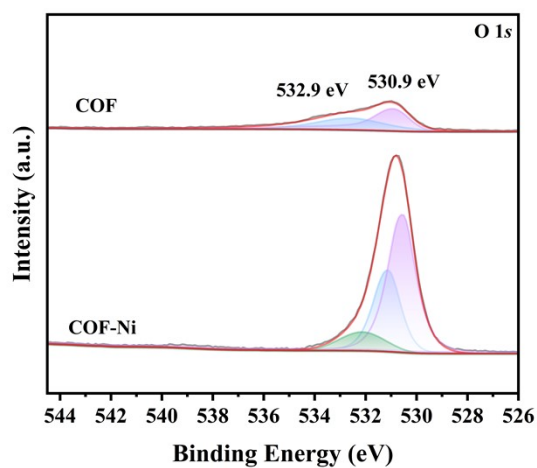


Figure S2. High-resolution O 1s XPS spectra of COF and COF-Tp-Azo-Ni_{0.33}.

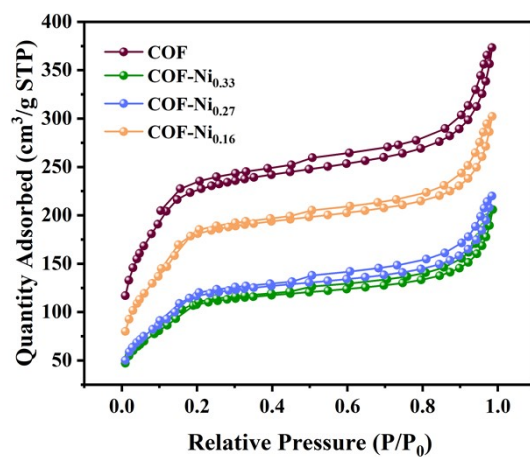


Figure S3. N₂ adsorption-desorption isotherms.

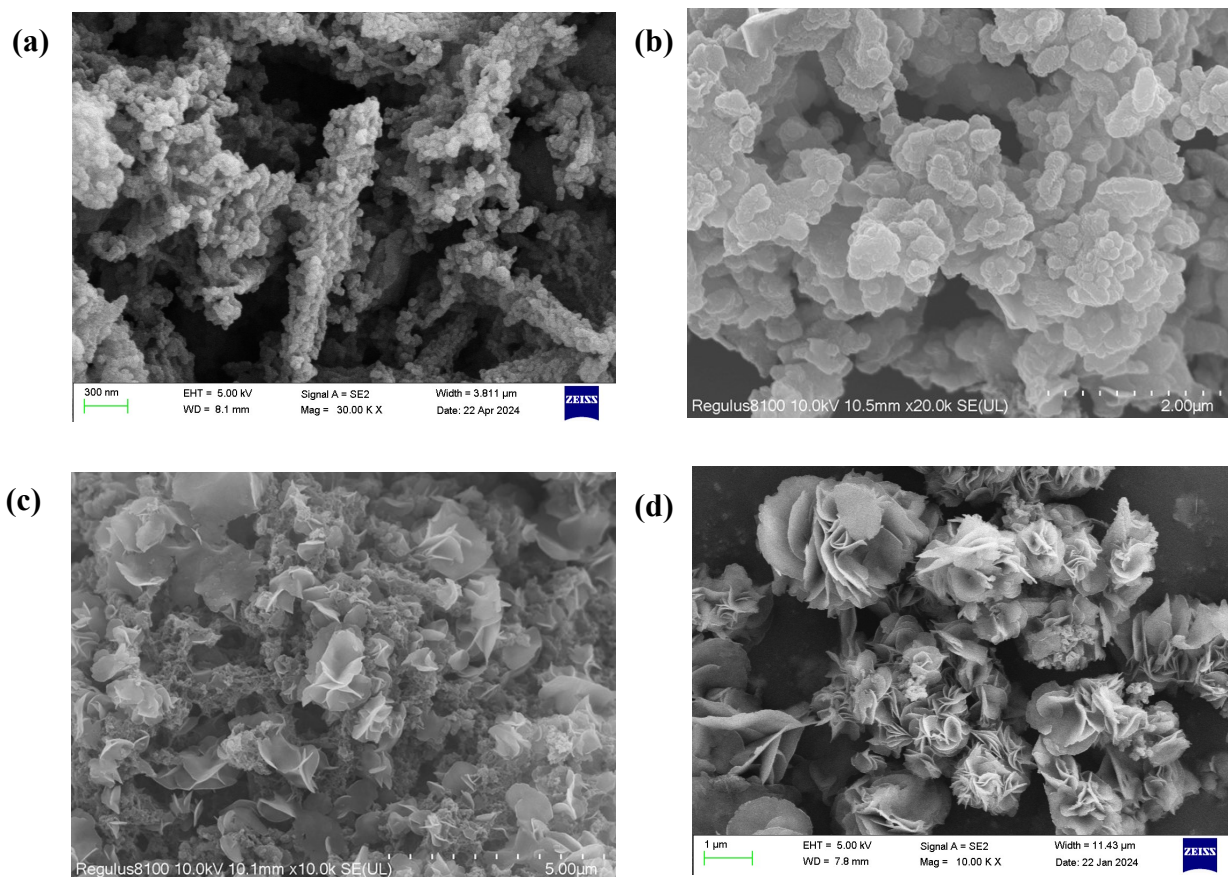


Figure S4. SEM images for (a) COF (b) COF-Tp-Azo-Ni_{0.16} (c) COF-Tp-Azo-Ni_{0.27} (d) COF-Tp-Azo-Ni_{0.33}.

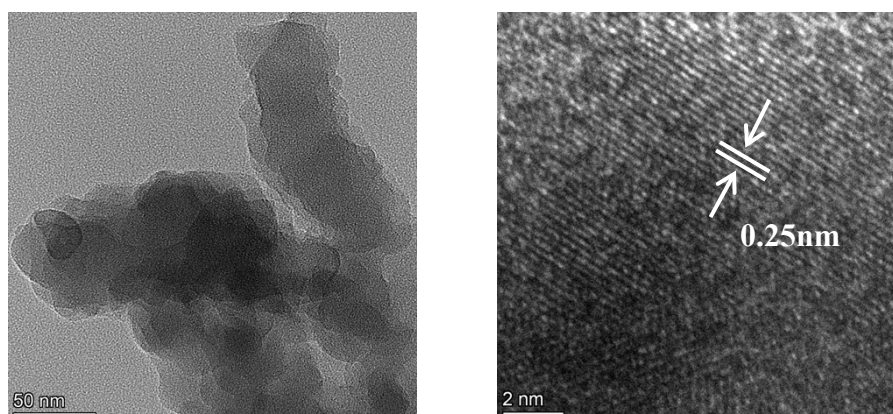


Figure S5. High resolution TEM images maps of COF-Tp-Azo.

(b)

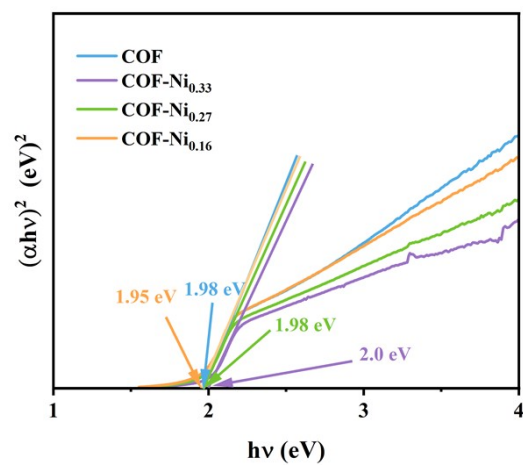
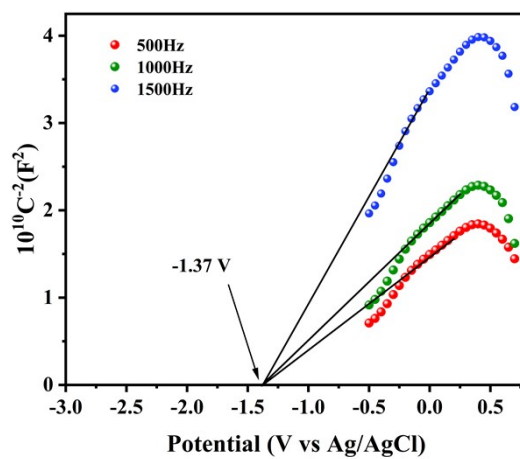
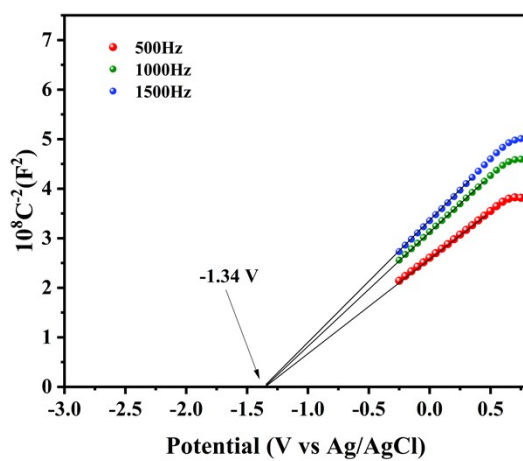


Figure S6. Tauc plots of COF-Tp-Azo-Ni_x for COF-Tp-Azo-Ni_x.



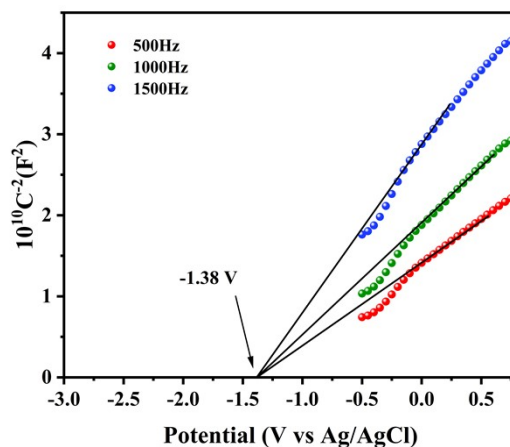


Figure S7. Mott-Schottky plots of COF-Tp-Azo-Ni_x at 500 Hz, 1000 Hz, and 1500 Hz measured in 0.2 M Na₂SO₄, with Ag/AgCl as the reference electrode. (a) COF-Tp-Azo-Ni_{0.33} (b) COF-Tp-Azo-Ni_{0.27} (c) COF-Tp-Azo-Ni_{0.16}.

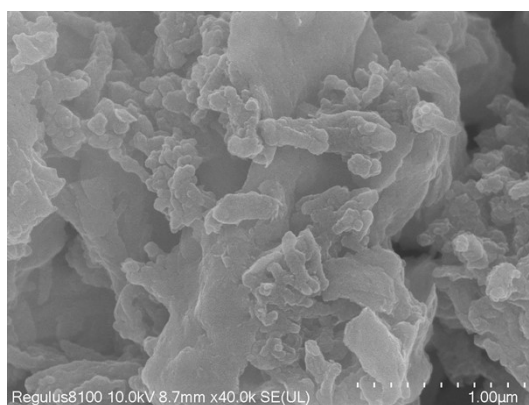


Figure S8. SEM image of COF-Tp-Azo-Ni_{0.16} after photocatalytic reaction in ACN/H₂O(v:v = 4:1) .

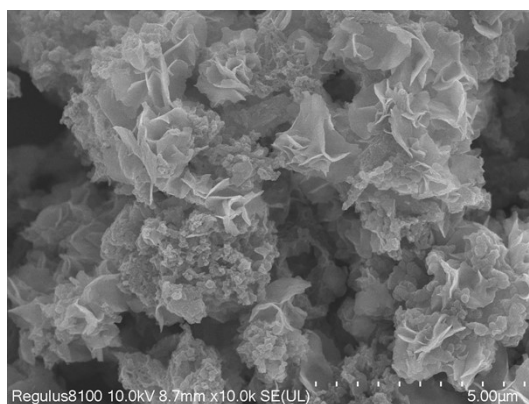


Figure S9. SEM image of COF-Tp-Azo-Ni_{0.27} after photocatalytic reaction in ACN/H₂O(v:v = 4:1) .

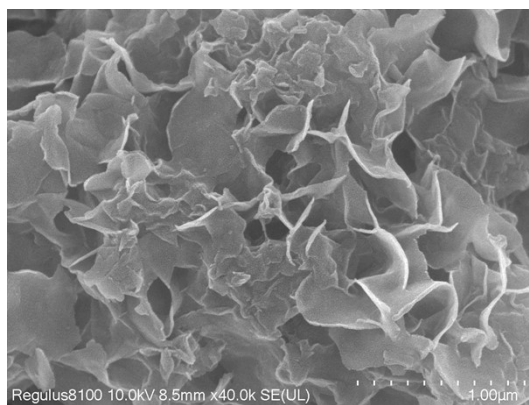


Figure S10. SEM image of COF-Tp-Azo-Ni_{0.33} after photocatalytic reaction in ACN/H₂O(v:v = 4:1) .

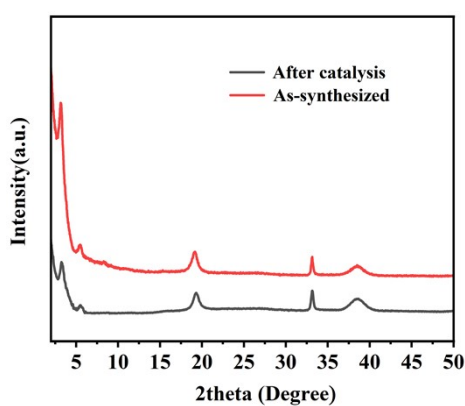


Figure S11. Powder XRD patterns of COF-Tp-Azo-Ni_{0.33} before and after photocatalytic reaction in ACN/H₂O (v:v = 4:1).

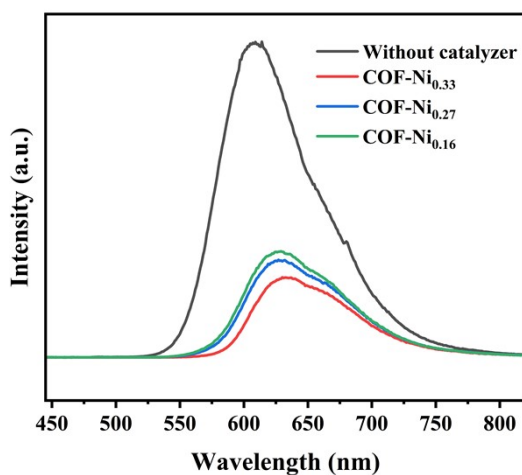


Figure S12. Photoluminescence spectra of [Ru(bpy)₃]Cl₂ in ACN/H₂O solutions containing the catalysts.

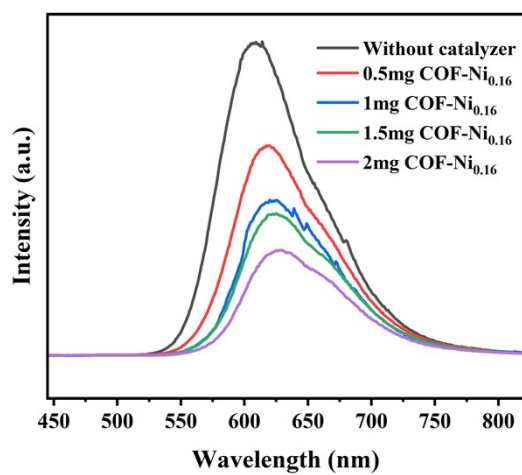
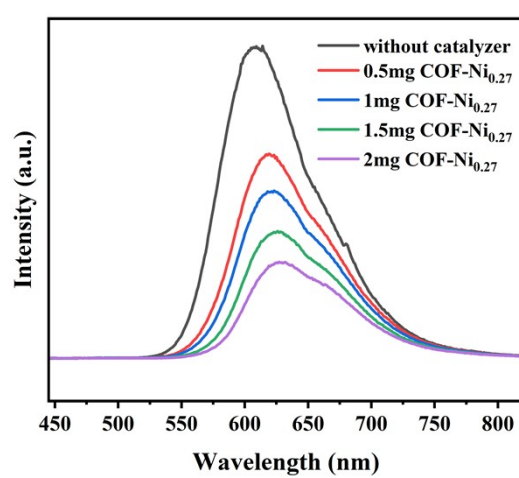
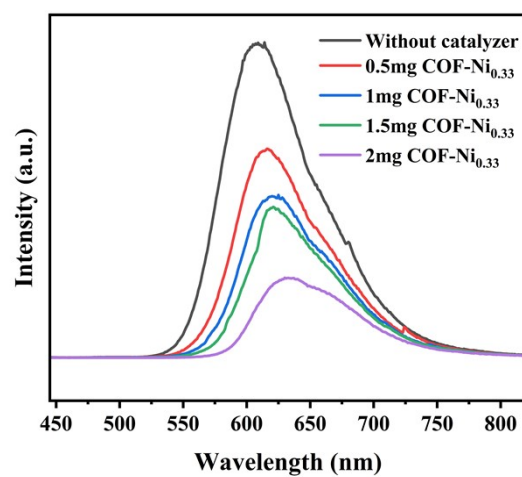


Figure S13. PL spectra of [Ru(bpy)₃]Cl₂ in ACN solution containing different contents of COF-Tp-Azo-Ni (0mg, 0.5mg, 1mg, 2mg) under excitation at 425 nm.

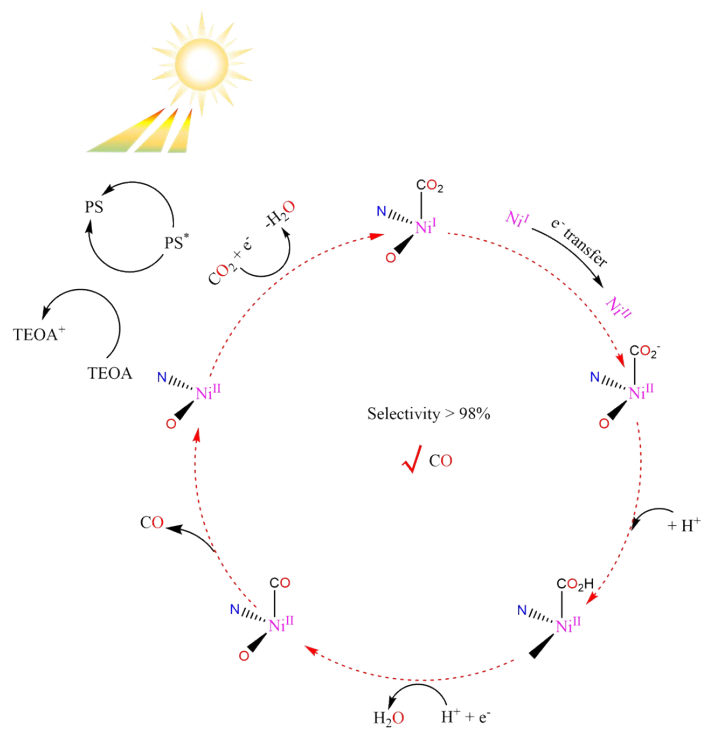


Figure S14. Proposed mechanism for CO₂ photoreduction into CO over COF-Tp-Azo-Ni.

Table S1. The results of control experiments for photocatalytic CO₂ reduction over Ni-COF-Tp-Azo_{0.33} in ACN / H₂O.

Entry	CO (mmol g ⁻¹)	CH ₄ (mmol g ⁻¹)	H ₂ (mmol g ⁻¹)	Selectivity to CO(%)
1	0	0	0	0
2	0	0	0	0
3	0	0	0	0
4	38.97	0	0.45	98.8

Entry 1: without [Ru(bpy)₃]Cl₂; Entry 2: without light; Entry 3: without TEOA; Entry 4: 100% CO₂. Reaction conditions: COF-Tp-Azo (2 mg), [Ru(bpy)₃]Cl₂ (22.5 mg), TEOA (2 mL), ACN (12 mL), H₂O (3 mL), Xe lamp ($\lambda > 420$ nm), 25 °C, 4 h.

Table S2. The results of control experiments for photocatalytic CO₂ reduction over Ni-COF-Tp-Azo_{0.33} in ACN / H₂O.

Entry	ACN/H ₂ O (V:V, V _{total} = 15 mL)	Products (mmol g ⁻¹)		Selectivity (%)	
		CO	H ₂	CO	H ₂
1	15 mL ACN	3.38	6.16	35.4	64.6
2	14:1	19.81	7.25	73.2	26.8
3	13:2	28.03	2.44	92.0	8.0
4	12:3	38.97	0.45	98.9	1.1
5	11:4	22.63	0.65	97.2	2.8
6	10:5	21.27	0.43	98.0	2.0
7	9:6	17.44	0.147	99.2	0.8

Table S3. The results of control experiments for photocatalytic CO₂ reduction over Ni-COF-Tp-Azo_{0.27} in ACN / H₂O.

Entry	ACN/H ₂ O (V:V, Vtotal = 15 mL)	Products (mmol g ⁻¹)		Selectivity (%)	
		CO	H ₂	CO	H ₂
1	15 mL ACN	5.52	3.46	61.5	38.5
2	14:1	14.16	0.88	94.1	5.9
3	13:2	17.23	1.50	92.0	8.0
4	12:3	24.15	0.98	96.1	3.9
5	10:5	25.08	0.40	98.4	1.6
6	9:6	6.08	0	100.0	0.0
7	8:7	5.50	0	100.0	0.0
8	1:1	4.22	3.02	58.3	41.7

Table S4. The results of control experiments for photocatalytic CO₂ reduction over Ni-COF-Tp-Azo_{0.16} in ACN / H₂O.

Entry	ACN/H ₂ O (V:V, Vtotal = 15 mL)	Products (mmol g ⁻¹)		Selectivity (%)	
		CO	H ₂	CO	H ₂
1	15 mL ACN	5.29	3.04	63.5	36.5
2	14:1	14.78	3.53	80.7	19.3
3	13:2	18.58	1.99	90.3	9.7
4	12:3	20.43	0.85	96.0	4.0
5	10:5	22.40	0.41	98.2	1.8
6	9:6	4.85	0	100.0	0.0
7	8:7	1.63	0	100.0	0.0

Table S5. Comparison of catalytic CO₂ photoreduction properties of different Ni metal-supported covalent organic framework materials.

Catalyst	Photosensitizers/ Sacrificial agent	Reaction solvent	CO ₂ reduction selectivity	CO ($\mu\text{mol g}^{-1} \text{h}^{-1}$)	Irradiation condition	Ref
Tp-Azo-Ni	[Ru(bpy) ₃]Cl ₂ TEOA	ACN/H ₂ O	98%	9743	$\lambda \geq 420 \text{ nm}$ (300 W Xe lamp)	This work
Ni-TP-CON	[Ru(bpy) ₃]Cl ₂ TEOA	ACN/H ₂ O	95%	4360	$\lambda \geq 420 \text{ nm}$ (300 W Xe lamp)	1
Ni-TPBpy	[Ru(bpy) ₃]Cl ₂ TEOA	ACN/H ₂ O	76%	228	$\lambda \geq 420 \text{ nm}$ (300 W Xe lamp)	2
Ni@TPHH-COF	[Ru(bpy) ₃]Cl ₂ TEOA	ACN/H ₂ O	96%	1610	$\lambda \geq 420 \text{ nm}$ (300 W Xe lamp)	3
NiP-TPE-COF	[Ru(bpy) ₃]Cl ₂ TEOA	ACN/H ₂ O	93%	525	$\lambda \geq 420 \text{ nm}$ (300 W Xe lamp)	4
TTCOF-Ni	--	H ₂ O	100%	0.08	$\lambda \geq 420 \text{ nm}$ (300 W Xe lamp)	5
Ni-PCD@TD- COF	[Ru(bpy) ₃]Cl ₂ TEOA	ACN/H ₂ O	82%	160	$\lambda \geq 420 \text{ nm}$ (300 W Xe lamp)	6
Ni@PI-COF-TT	2'2-bipyridine TEOA	ACN/H ₂ O	93%	483	$\lambda \geq 420 \text{ nm}$ (300 W Xe lamp)	7
PD-COF-23-Ni	TEOA	ACN/H ₂ O	99%	40	$\lambda \geq 420 \text{ nm}$ (300 W Xe lamp)	8
(H-COF-Ni)	[Ru(bpy) ₃]Cl ₂ TEOA	ACN/H ₂ O	96%	1958	$\lambda \geq 420 \text{ nm}$ (300 W Xe lamp)	9
Ni-TPTG _{Cl}	[Ru(bpy) ₃]Cl ₂ TEOA	ACN/H ₂ O	92%	8600	LED light (420 nm < λ < 800 nm)	10
EPNi-COF	[Ru(bpy) ₃]Cl ₂ TEOA	ACN/H ₂ O	74%	1000	$\lambda \geq 420 \text{ nm}$ (300 W Xe lamp)	11
OMHS-COF-Ni	[Ru(bpy) ₃]Cl ₂ TIPA	ACN/H ₂ O	99%	2600	$\lambda \geq 420 \text{ nm}$ (300 W Xe lamp)	12
Ni-PyPor-COF	[Ru(bpy) ₃]Cl ₂ TEOA	ACN/H ₂ O	84%	4520	$\lambda \geq 420 \text{ nm}$ (300 W Xe lamp)	13
Ni SAS/Tr-COF	[Ru(bpy) ₃]Cl ₂ TEOA	ACN/H ₂ O	90%	335	$\lambda \geq 420 \text{ nm}$ (300 W Xe lamp)	14

NiPor-BDOB	[Ru(bpy) ₃]Cl ₂ TEA	ACN/H ₂ O	97%	1770	$\lambda \geq 420$ nm (300 W Xe lamp)	15
ETTA-Bpy-COF-Ni	[Ru(bpy) ₃]Cl ₂ TIPA	ACN/H ₂ O	99%	1850	$\lambda \geq 420$ nm (300 W Xe lamp)	16

References:

- (1) H.-W. Lv, P.-Y. Li, X.-J. Li, A.-C. Chen, R.-J. Sa, H. Zhu and R.-H. Wang, Boosting photocatalytic reduction of the diluted CO₂ over covalent organic framework, *Chem. Eng. J.*, 2023, **451**, 138745.
- (2) W.-F. Zhong, R.-J. Sa, L.-Y. Li, Y.-J. He, L.-Y. Li, J.-J. Bi, Z.-Y. Zhuang, Y. Yu and Z.-G. Zou, A Covalent Organic Framework Bearing Single Ni Sites as a Synergistic Photocatalyst for Selective Photoreduction of CO₂ to CO, *J. Am. Chem. Soc.*, 2019, **141**, 7615-7621.
- (3) M. Dong, J. Zhou, J. Zhong, H.-T. Li, C.-Y. Sun, Y.-D. Han, J.-N. Kou, Z.-H. Kang, X.-L. Wang and Z.-M. Su, CO₂ Dominated Bifunctional Catalytic Sites for Efficient Industrial Exhaust Conversion, *Adv. Funct. Mater.*, 2021, **32**, 2110136.
- (4) H.-W. Lv, R.-J. Sa, P.-Y. Li, D.-Q. Yuan, X.-C. Wang and R.-H. Wang, Metalloporphyrin-based covalent organic frameworks composed of the electron donor-acceptor dyads for visible-light-driven selective CO₂ reduction, *Science China Chemistry*, 2020, **63**, 1289-1294.
- (5) M. Lu, J. Liu, Q. Li, M. Zhang, M. Liu, J.-L. Wang, D.-Q. Yuan and Y.-Q. Lan, Rational Design of Crystalline Covalent Organic Frameworks for Efficient CO₂ Photoreduction with H₂O, *Angew. Chem., Int. Ed.*, 2019, **58**, 12392-12397.
- (6) H. Zhong, R.-J. Sa, H.-W. Lv, S.-L. Yang, D.-Q. Yuan, X.-C. Wang and R.-H. Wang, Covalent Organic Framework Hosting Metalloporphyrin-Based Carbon Dots for Visible-Light-Driven Selective CO₂ Reduction, *Adv. Funct. Mater.*, 2020, **30**, 2002654.
- (7) X. Chen, Q. Dang, R.-J. Sa, L.-Y. Li, L. Li, J.-H. Bi, Z.-Z. Zhang, J.-L. Long, Y. Yu and Z.-G. Zou, Integrating single Ni sites into biomimetic networks of covalent organic frameworks for selective photoreduction of CO₂, *Chem Sci.*, 2020, **11**, 6915-6922.
- (8) N.-F. Xu, Y.-X. Diao, X.-H. Qin, Z.-T. Xu, H.-Z. Ke and X.-J. Zhu, Donor-acceptor covalent organic frameworks of nickel(II) porphyrin for selective and efficient CO₂ reduction into CO, *Dalton Trans.*, 2020, **49**, 15587-15591.
- (9) S.-L. Yang, R.-J. Sa, H. Zhong, H.-W. Lv, D.-Q. Yuan and R.-H. Wang, Microenvironments Enabled by Covalent Organic Framework Linkages for Modulating Active Metal Species in Photocatalytic CO₂ Reduction, *Adv. Funct. Mater.*, 2022, **32**, 2110694.
- (10) H.-B. Wu, W. Zou, S.-X. Shao, X.-T. Zhou, Z.-H. Zhou and Y.-X. Fang, Cobalt and nickel coordinated guanidinium-based two-dimensional covalent organic framework nanosheets for efficient photocatalytic CO₂ reduction, *Catalysis Today*, 2022, **402**, 202-209.
- (11) W. Lin, F.-W. Lin, J. Lin, Z.-W. Xiao, D.-Q. Yuan and Y.-B. Wang, Efficient Photocatalytic CO₂ Reduction in Ellagic Acid-Based Covalent Organic Frameworks, *J. Am. Chem. Soc.*, 2024, **146**, 16229-16236.
- (12) T.-Y. Zheng, X. Ding, T.-T. Sun, X.-Y. Yang, X.-X. Wang, X. Zhou, P.-P. Zhang, B.-Q. Yu, Y.-H. Wang, Q.-M. Xu, L.-B. Xu, D.-S. Wang and J.-Z. Jiang, Nanostructurally Engineering Covalent Organic Frameworks for Boosting CO₂ Photoreduction, *Small*, 2023, **20**, 2307743.

- (13) T.-X. Luan, J.-R. Wang, K. Li, H. Li, F. Nan, W.-W. Yu and P.-Z. Li, Highly Enhancing CO₂ Photoreduction by Metallization of an Imidazole-linked Robust Covalent Organic Framework, *Small*, 2023, **19**, 2303324.
- (14) L. Ran, Z.-W. Li, B. Ran, J.-Q. Cao, Y. Zhao, T. Shao, Y.-R. Song, M. K. H. Leung, L.-C. Sun and J.-G. Hou, Engineering Single-Atom Active Sites on Covalent Organic Frameworks for Boosting CO₂ Photoreduction, *J. Am. Chem. Soc.*, 2022, **144**, 17097-17109.
- (15) S. Suleman, K. Sun, Y. Zhao, X. Guan, Z. Lin, Z. Meng and H.-L. Jiang, Enhanced Photocatalytic CO₂ Reduction via Linkage Substitution in Porphyrinic Covalent Organic Frameworks, *CCS Chem.*, 2024, **6**, 1689-1697.
- (16) Y.-H. Wang, T.-T. Sun, T.-Y. Zheng, X. Ding, P.-P. Zhang, Q.-M. Xu, T.-X. Li, S.-L. Zhang, K. Wang, L.-B. Xu and J.-Z. Jiang, Two-Dimensional Kagome Covalent Organic Frameworks with Single Atomic Co Sites for Superior Photocatalytic CO₂ Reduction, *ACS Mater. Lett.*, 2023, **6**, 140-152.